Evaluation of cloudless-sky periods detected by shortwave and longwave algorithms using lidar measurements

Jean-Charles Dupont, Martial Haeffelin, Charles N. Long

Evaluation of cloudless-sky periods detected by shortwave and longwave algorithms using lidar measurements

Jean-Charles Dupont,[1] Martial Haeffelin,[2] and Charles N. Long[3]

Received 28 February 2008; revised 11 April 2008; accepted 23 April 2008; published 30 May 2008.

[1] Identifying cloud-free periods is important as they are used as common references in cloud and aerosol radiative forcing studies. Their identification requires precise methods to distinguish condensed water from other aerosols (e.g. mineral or moist hydrophilic aerosols). In this study we combine analyses of wide field of view shortwave (SW) and longwave (LW) irradiances and Lidar backscatter measurements to explore situations that are considered neither completely clear nor cloudy. We find that situations classified as cloud-free by analysis of SW (LW) measurements are also classified as cloud free by the Lidar in more than 60% (50%) of situations. The remaining 40% (50%) situations are classified as cloudy by the Lidar, and are hence considered as hazy. These hazy situations are predominantly composed of high-altitude cirrus clouds, partitioned equally between subvisible and semi-transparent optical thickness classes. We find that, in hazy situations, the average cloud radiative forcing on surface SW irradiances ranges between -5 and -15 Wm^{-2}.
Citation: Dupont, J.-C., M. Haeffelin, and C. N. Long (2008), Evaluation of cloudless-sky periods detected by shortwave and longwave algorithms using lidar measurements, *Geophys. Res. Lett.*, *35*, L10815, doi:10.1029/2008GL033658.

1. Introduction

[2] Radiative effects of clouds and aerosol play an important and complex role in the balance of the Earth's energy. They are quantified by the Cloud Radiative Forcing (CRF) and by the Aerosol Radiative Forcing (ARF) and are defined as the differences between all-sky and cloud-free situations and between cloud-free and pristine situations, respectively. Reliable detection of condensed water or ice in the atmospheric column is essential to precisely quantify each radiative forcing and to distinguish ARF from CRF. Accurate estimations of ARF and CRF rely on precise identification of cloud free references. The relatively high abundance of high altitude optically thin clouds [*Chen et al.*, 2000], characterized by a signature that is difficult to detect (small instantaneous radiative impact, low concentration in particles, non-visible), is likely to disturb the cloud-free reference identification. In surface and top-of-the-atmosphere CRF studies [*Chen et al.*, 2000; *Shupe and Intrieri*, 2003; *Dong et al.*, 2006; *Mace et al.*, 2006], cloud free references are based on different detection techniques. Hence, the results of these studies depend to some extent on the observing means used to classify the sky as cloud free.

[3] Cloud free periods can be identified either by human observers or by active and passive instruments. Identification errors reach almost 50% for high altitude clouds [*Rodriguez*, 1998]. For instance, human observations are subjective and have a limited temporal and spatial resolution. Active instruments like lidars and ceilometers have a limited field of view [*Nadolski*, 1995], while passive instruments like hemispheric sky imagers [*Long et al.*, 2006a] often experience difficulties correctly determining the presence of clouds near the sun. Additionally, the availability of lidar, ceilometer, and sky imager data has been limited to date. Hence, automatic algorithms using either shortwave or longwave downwelling irradiance were developed to optimize and generalize the detection of clouds.

[4] In this paper, we first evaluate the cloud detection sensitivity provided by two different methods, one using the longwave downwelling irradiance and one using the shortwave downwelling irradiance, against collocated lidar measurements. Next, we quantify the macrophysical and microphysical properties and radiative impact of the amounts of condensed water or ice in the atmosphere that traditionally have not been classified as "clouds" by observers, sky imagers, or the longwave and shortwave algorithms.

2. Observation Data Set

[5] The SIRTA (Site Instrumental de Recherche par Télédétection Atmosphérique) observatory is located in a semi-urban area, 25 km south of Paris (48.7 N, 2.2 E). The observatory gathers active and passive remote sensing data dedicated to describing the atmospheric column in terms of clouds and aerosols since 2002 [*Haeffelin et al.*, 2005].

[6] Irradiance measurements are acquired on the observatory rooftop platform to provide an optimal view for these hemispheric field-of-view instruments. SIRTA is part of the Baseline Surface Radiation Network (BSRN) [*Ohmura et al.*, 1998] which strives to ensure continuous high quality, highly sampled (0.2-Hz sampling, 1-min average) solar and infrared irradiance. Shortwave direct and diffuse downwelling irradiances (0.3 to 4.0 μm) are measured at SIRTA using Kipp and Zonen instruments, a CH1 pyrheliometer and a shaded CM22 pyranometer, respectively. These two components are then combined to provide the total downwelling shortwave irradiance [*Ohmura et al.*, 1998]. Longwave downwelling irradiances (4.5 to 42 μm) are measured using a shaded Kipp and Zonen CG4 pyrgeometer [*Haeffelin et al.*, 2005].

[7] The SIRTA Observatory deploys a dual wavelength depolarization lidar, Lidar Nuages Aerosols, (LNA, Cloud

[1]Institut Pierre Simon Laplace, Laboratoire de Météorologie Dynamique, Ecole Polytechnique, Palaiseau, France.
[2]Institut Pierre Simon Laplace, Ecole Polytechnique, Palaiseau, France.
[3]Atmospheric Radiation Measurement Program, Pacific Northwest National Laboratory, Richland, Washington, USA.

0094-8276/08/2008GL033658

and Aerosol Lidar). Vertical resolution is 15 m and the detected wavelengths are 532 nm (parallel and cross polarized) and 1064 nm [*Haeffelin et al.*, 2005]. The LNA backscattered signal provides information on the presence of clouds and aerosols in the vertical column between 0.5 and 15 km altitude. A multiple test algorithm [*Morille et al.*, 2007] is applied to the 532 and 1064 nm linear polarization channels to retrieve the vertical distribution of cloud and aerosol layers in the boundary layer and through the free troposphere and to identify near-particle-free regions in the vertical profile and the range at which the lidar signal becomes too attenuated for exploitation. The cloud mask provided by this algorithm is then analyzed to estimate Cloud Base Height (CBH), Cloud Top Height (CTH) and time series Cloud Fraction (CF). When the lidar is able to penetrate through the entire depth of the cloud (range flag at higher altitude than CTH), the lidar backscatter below and above the cloud is used to estimate the total cloud attenuation, or Cloud Optical Thickness (COT) using well documented methods [e.g., *Cadet et al.*, 2005].

3. Cloud-Free Period Detection and Evaluation

[8] For this study, we define the term "cloud-free" to mean a sky without any condensed liquid or ice water for all classes of altitude (low, medium and high). Note that for this study, we fix the lidar lower cloud detection limit to be 0.01 optical thickness. *Long et al.* [2006b] have developed algorithms to calculate cloud amount, noted CF, based on shortwave irradiance measurements. CF estimated by the shortwave algorithm (SWA), hereinafter referred to as CFSW, is limited to times with a solar elevation angle of 10° or greater [*Long and Ackerman*, 2000; *Sutter et al.*, 2004]. The cloud-free periods derived from SWA correspond to times where cloud influence on the magnitude and variability of the broadband total downwelling SW irradiance at the surface is significantly smaller than measurement uncertainty. CF can also be estimated based on analysis of surface downwelling longwave irradiance measurements [*Marty and Philipona*, 2000; *Dürr and Philipona*, 2004]. Cloud-free periods detected by the longwave flux algorithm (LWA) in this study are based on analysis of downwelling longwave irradiance standard deviation for a ±10-minute period centered on the time of interest. The maximum allowed standard deviation for a cloud-free situation is 1.1 W m^{-2}. LWA can be applied round-the-clock.

[9] Time series cloud fraction derived by temporal integration of backscattered lidar signal (time period of 60 minutes) is noted CFLI [*Morille et al.*, 2007]. This lidar algorithm (LIA) is intended to provide a reference for cloud-free periods since the lidar is sensitive to all condensed water layers (water and ice) with COT greater than 0.01. However, the LIA is insensitive to the clouds outside the very narrow beam, whereas the longwave and shortwave algorithms [*Sutter et al.*, 2004] are effectively sensitive to about a 160° field of view (FOV). We use a 1-hour temporal integration of lidar data to better represent the 160° FOV. For cirrus clouds at an average altitude of 10 km and a wind speed of 20 m s^{-1}, a 1-hour integration is roughly equivalent to a 150° 2D slice through the hemispheric FOV and to first order comparable to the SWA and LWA FOV. However, this calculation assumes that the cloud field is evenly distributed across the hemisphere, and that the cloud field is static, i.e. the cloud field morphology is far less significant than the cloud movement during the integration time. As *Kassianov et al.* [2004] show, for a static cloud field of 30% cloud fraction, a 15-minute narrow FOV slice thorough the field such as that of the lidar produces a time series cloud fraction value from 20% to 40% only about 20% of the time. The other 80% of the time the lidar-derived cloud fraction differs from reality by more than 10% cloud fraction amount. Hence in this study, LIA is not used to compute an exact reference cloud fraction. However, when LIA identifies a cloud (CFLI $\neq$ 0), we can be sure that there is a cloud element somewhere in the 160° FOV. So, the Lidar information is used to study what cloud properties define the more typical cloud/no cloud limit commonly defined by irradiance measurements and human observations.

[10] The dataset contains 22000 hours of radiometer measurements in 2003–2006 with about 700 hours of coincident Lidar measurements. Coincident measurements occur 90% during daytime and 10% during nighttime. The Lidar is only operated when the risk of precipitation is small, hence coincident Lidar/radiometer observations are biased towards a greater number of cloud-free situations and a lesser number of overcast situations, when compared to all observations. Table 1 shows occurrences (%) of CFLI for both CFSW = 0% and CFLW = 0%, based on analysis of coincident measurements only. Table 1 shows separate analysis for daytime and nighttime when CFLW = 0. In Table 1, cloud-free periods correspond to CF = 0% and overcast to CF = 100%. Table 1 reveals that identification of cloud-free situations by SWA (CFSW = 0%) is in agreement with LIA 68% of the time. In the remaining 32%, LIA identifies 31 % broken clouds and 1% overcast situations. Similarly Table 1 reveals that, during daytime (nighttime), identification of cloud-free situations by LWA (CFLW = 0%) is in agreement with LIA 51% (54%) of the time. In the remaining situations where LWA says it is cloud free, LIA frequently identifies an overcast situation both during daytime and nighttime. Table 1 confirms that a large part of the disagreements is due to broken cloud situations. Next we analyze the properties of clouds detected by the Lidar coincident with situations detected as cloud-free by SWA and LWA.

4. Macrophysical Properties of Residual Clouds

[11] In this study, the term "residual clouds" is defined as the clouds detected by LIA and not detected by SWA and/or LWA. Hence, in the cloud/no cloud limit domain, we classify the sky in three classes: unambiguously cloud-free (CFLI = CFLW = CFSW = 0%), unambiguously cloudy (CFLI > 0%, CFLW > 0%, CFSW > 0%), and "hazy" (CFLI > 0%, CFLW = 0% or CFSW = 0%). We focus our attention here on hazy cases where cloud radiative impact is difficult to measure and to distinguish from dry aerosol impact. Figure 1 shows the cloud occurrences according to CFLI, when CFLW or CFSW equals 0%, binned at 12.5% intervals for daytime (A and B) and nighttime periods (C). In daytime situations detected as cloud-free by SWA and LWA, 32% and 49 % are identified as cloudy by LIA (CFLI > 0%), respectively. Hence, those situations fall in the "hazy" class. During

Table 1. Occurrences of CFLI (Clear-Sky, Broken Clouds, Overcast Periods) for CFSW = 0%, Daytime CFLI for CFLW = 0%, and Nighttime CFLI for CFLW = 0%

	CFSW = 0% Day, %	CFLW = 0% Day, %	CFLW = 0% Night, %
Cloud-free (CFLI = 0%)	**68**	**51**	**54**
Broken-clouds (CFLI>0% and CFLI<100%)	31	36	26
Overcast (CFLI = 100%)	1	13	20

nighttime periods (LWA only), the hazy class occurs in 46 % of situations. Daylight hazy cases are composed of broken clouds 97% of the time for SWA and 73% of the time for LWA, respectively (56 % during nighttime periods).

[12] Figures 1d, 1e, and 1f display the vertical distribution of cloud occurrence based on LIA with each box representing a 20% step of CFLI at 1 km vertical resolution. "Hazy SWA" situations are predominantly (80%) characterized by broken clouds with cloud base heights in the 8–12 km range. Since the SW method equates the enhancement of the diffuse SW to cloud amount, this upper level cloudiness likely exhibits thin optical depth characteristics that only somewhat increase the diffuse SW. "Hazy LWA" situations are characterized by overcast clouds at both high and low altitudes (50% CBH < 8 km) and by broken clouds predominantly at high altitude. Overcast clouds may be associated with small variations in the longwave irradiance time series, while high altitude clouds do not significantly increase the surface downwelling LW.

5. Optical and Radiative Properties of Residual Clouds

[13] Residual clouds which correspond to hazy cases can be classified according to their cloud optical thickness (COT). We divide these into 3 classes: subvisibles (COT < 0.03), semi-transparents (0.03 < COT < 0.3) or moderate (COT > 0.3).

[14] The retrieval method to process cloud optical thickness, molecular integration (MI), estimates the backscatter attenuation between the observed lidar return above the cloud top and the theoretical molecular lidar return in the absence of cloud [*Cadet et al.*, 2005]. This requires a significant signal-to-noise ratio above the given layer, hence only layers that are penetrated all the way through by the lidar are considered (i.e. with a cloud optical thickness ranging from 0 to 3). Figure 2 shows the cumulative occurrence of COT for the residual cases associated with LWA and/or SWA equal to 0%. These cases are optically thicker for CFLW = 0% than for CFSW = 0%. For the LW algorithm during daytime periods 30% of the occurrences are subvisibles (12% for nighttime periods), 64% semi-transparents (70% nighttime) and 6% moderate (18% nighttime). Residual cases associated with SWA are 40% subvisibles and 60% semi-transparents. SWA is more sensitive to optically thin cases than LWA, as roughly 95% of the cases fall below a COT of about 0.15, and virtually 100% of optically moderate cases are screened.

[15] Cloud/no cloud for the SW technique is to first order based on the impact on the total downwelling SW irradiance. Low level clouds, which tend to be optically thicker, engender a significant attenuation of the SW direct irradiance which is not completely compensated by the increase of SW diffuse irradiance. However, for high level and optically thin clouds (COT < 0.15), surface downwelling SW total irradiance is generally not significantly affected since what is scattered out of the direct is mostly forward scattered and thus is partitioned into the downwelling diffuse. To illustrate this point, we estimate the radiative impact of clouds not detected by SWA and/or LWA. This cloud radiative impact (CRF_{SW}) is computed as the difference between the measured SW irradiance and a reference

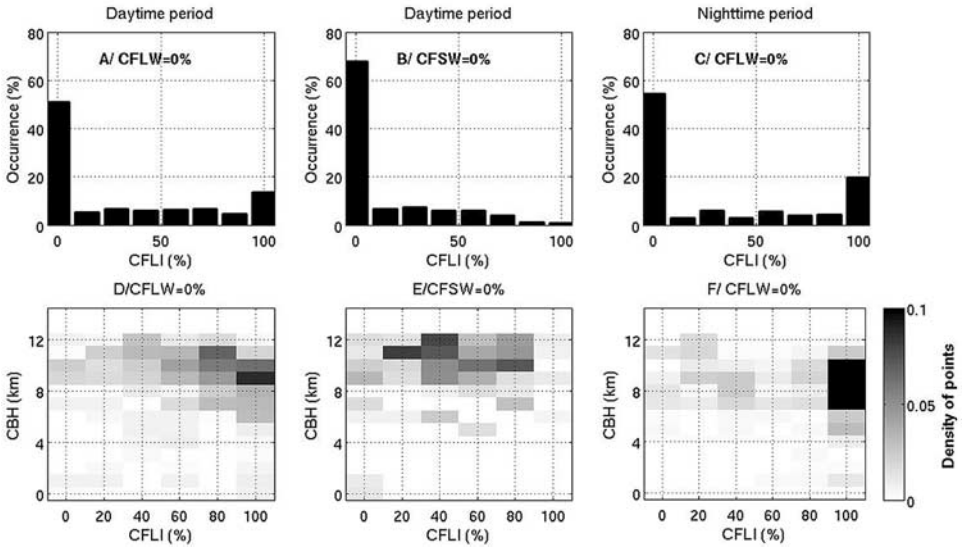

Figure 1. (a) and (b) The occurrence frequencies of CFLI during daytime periods for CFLW = 0% and CFSW = 0%. (c) Distribution of CFLI during nighttime periods for CFLW = 0%. (d)-(f) The 2D-plots of CFLI by altitude for the hazy cases.

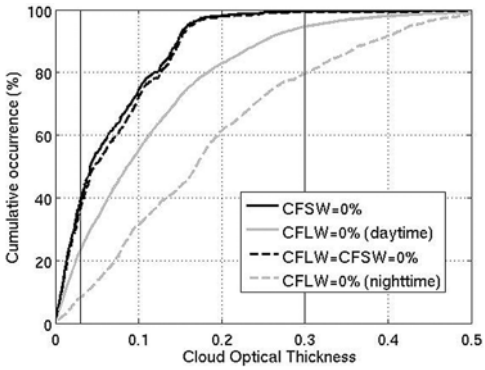

Figure 2. Cumulative occurrence of the cloud optical thickness during hazy situations. Vertical lines correspond to class limit of subvisible and semi-transparents cirrus clouds.

cloud-less sky SW irradiance value ($SW_{cldless}$). $SW_{cldless}$ is estimated based on a parametric model [*Dutton et al.*, 2004]. This model is fitted to the cloudless-sky periods detected by the three algorithms: CFSW = CFLW = CFLI = 0%. For those situations we find a mean $CRF_{SW} = 0$ W m^{-2}, with a root mean square error of 5.5 W m^{-2}. For "hazy SWA" situations (CFLI > 0% and CFSW = 0%), we find a mean $CRF_{SW} = -6$ W m^{-2}, while for "hazy LWA" situations (CFLI > 0% and CFLW = 0%) the mean $CRF_{SW} = -16$ W m^{-2}. This confirms that residual clouds not detected by LWA have a more significant impact on solar irradiances than residual clouds not detected by SWA.

6. Conclusion

[16] Cloud-free periods detected by an analysis of shortwave and longwave irradiance time series are evaluated against lidar detections of condensed water or ice in the column. Agreement in identification of cloud-free periods between LIA and SWA (LWA) occurs 32% (51–54%) of the time. The residual occurrences detected by the lidar but not classified as "cloudy" by the broadband techniques is composed of 90% high cirrus clouds for SWA (80% for LWA), and classified in terms of cloud optical thickness as 40% subvisible (20%), 59% semi-transparent (74%) and 1 % moderate (6%). The average altitude of residual cloud cases not classified as cloud by SWA is about 9.5 km (8.5 km for LWA). These cold, high and optically thin clouds have an average radiative impact near -5 Wm^{-2} (-15 Wm^{-2} for LWA) out of 375 Wm^{-2} total SW irradiance. The broadband techniques cannot by themselves detect occurrences of situations where there is virtually no condensed water in the atmospheric column, i.e. times that are considered "hazy" but still "cloud free" by general definition, and distinguish these occurrences from what is typically considered dry aerosols. Thus, a combined analysis of both passive and active remote sensing instruments seems essential to precisely detect totally haze-free cloud-free periods.

[17] The sensitivity of SWA and LWA in terms of optical thickness shows that in general the SW algorithm effectively produces a "cloud free" definition for optical depths of 0.15 and less (0.3 and less for the LW algorithm, with the caveat that high clouds are not detected). In general it is higher altitude cases that are not detected by SWA or LWA. These cases, defined as sub-visual to semi-transparent cirrus, have only a small radiative impact at the surface. But in light of the current interest in aerosol direct and indirect effects, their cumulative impact on the radiative budget and separation from aerosol effects alone can be significant.

[18] **Acknowledgments.** The authors would like to thank the Centre National d'Etudes Spatiales (CNES), the Centre National de la Recherche Scientifique (CNRS) and the Climate Change Research Division of the U.S. Department of Energy as part of the Atmospheric Radiation Measurement (ARM) Program for their support in this study. The authors are grateful to the anonymous reviewers for their useful comments.

References

Cadet, B., V. Giraud, M. Haeffelin, P. Keckhut, A. Rechou, and S. Baldy (2005), Improved retrievals of the optical properties of cirrus clouds by a combination of lidar methods, *Appl. Opt.*, *44*, 1726–1734.

Chen, T., W. B. Rossow, and Y. Zhang (2000), Radiative effects of cloud-type variations, *J. Clim.*, *13*, 264–286.

Dong, X., B. Xi, and P. Minnis (2006), A climatology of midlatitude continental clouds from the ARM SGP central facility. Part II: Cloud fraction and surface radiative forcing, *J. Clim.*, *19*, 1765–1783.

Dürr, B., and R. Philipona (2004), Automatic cloud amount detection by surface longwave downward radiation measurements, *J. Geophys. Res.*, *109*, D05201, doi:10.1029/2003JD004182.

Dutton, E. G., A. Farhadi, R. S. Stone, C. N. Long, and D. W. Nelson (2004), Long-term variations in the occurrence and effective solar transmission of clouds as determined from surface-based total irradiance observations, *J. Geophys. Res.*, *109*, D03204, doi:10.1029/2003JD003568.

Haeffelin, M., et al. (2005), SIRTA, a ground-based atmospheric observatory for cloud and aerosol research, *Ann. Geophys.*, *23*, 262–275.

Kassianov, E., C. N. Long, and M. Ovtchinnikov (2004), Cloud sky cover versus cloud fraction: Whole-sky simulations and observations, *J. Appl. Meteorol.*, *44*, 86–98.

Long, C. N., and T. P. Ackerman (2000), Identification of clear skies from broadband pyranometer measurements and calculation of downwelling shortwave cloud effect, *J. Geophys. Res.*, *105*, 609–625.

Long, C. N., J. M. Sabburg, J. Calbo, and D. Pages (2006a), Retrieving cloud characteristics from ground-based daytime color all-sky images, *J. Atmos. Oceanic Technol.*, *23*, 633–652.

Long, C. N., T. P. Ackerman, K. L. Gaustad, and J. N. S. Cole (2006b), Estimation of fractional sky cover from broadband shortwave radiometer measurements, *J. Geophys. Res.*, *111*, D11204, doi:10.1029/2005JD006475.

Mace, G., S. Benson, and S. Kato (2006), Cloud radiative forcing at the Atmospheric Radiation Measurement Program Climate Research Facility: 2. Vertical redistribution of radiant energy by clouds, *J. Geophys. Res.*, *111*, D11S91, doi:10.1029/2005JD005922.

Marty, C., and R. Philipona (2000), The clear-sky index to separate clear-sky situations in climate research, *Geophys. Res. Lett.*, *27*, 1641–1644.

Morille, Y., M. Haeffelin, P. Drobinski, and J. Pelon (2007), STRAT: An automated algorithm to retrieve the vertical structure of the atmosphere from single-channel lidar data, *J. Atmos. Oceanic Technol.*, *24*, 761–775.

Nadolski, V. (1995), United States moves ahead with deployment of the Automated Surface Observing System, *ICAO J.*, *50*, 10–11.

Ohmura, A., et al. (1998), Baseline Surface Radiation Network (BSRN/WCRP): New precision radiometry for climate research, *Bull. Am. Meteorol. Soc.*, *79*, 2115–2136.

Rodriguez, D. (1998), On the comparability of cloud fractions derived from whole sky imager and ceilometer data, *Rep. UCRL-ID-129839*, Tech. Inf. Dep., Lawrence Livermore Natl. Lab., Livermore, Calif.

Shupe, M. D., and J. M. Intrieri (2003), Cloud radiative forcing of the Arctic surface: The influence of cloud properties, surface albedo, and solar zenith angle, *J. Clim.*, *17*, 616–628.

Sutter, M., B. Durr, and R. Philipona (2004), Comparison of two radiation algorithms for surface-based cloud-free sky detection, *J. Geophys. Res.*, *109*, D17202, doi:10.1029/2004JD004582.

J.-C. Dupont, Institut Pierre Simon Laplace, Laboratoire de Météorologie Dynamique, Ecole Polytechnique, F-91128 Palaiseau CEDEX, France. (jean-charles.dupont@lmd.polytechnique.fr)

M. Haeffelin, Institut Pierre Simon Laplace, Ecole Polytechnique, F-91128 Palaiseau CEDEX, France.

C. N. Long, Atmospheric Radiation Measurement Program, Pacific Northwest National Laboratory, P. O. Box 999, Richland, WA 99352, USA.